



Published in final edited form as:

Mater Res Bull. 2009 June ; 34(6): 415–421.

Gold-Based Magneto/Optical Nanostructures: Challenges for *In Vivo* Applications in Cancer Diagnostics and Therapy

Marites Melancon, Wei Lu, and Chun Li

Departments of Experimental Diagnostic Imaging, The University of Texas M. D. Anderson Cancer Center, Houston, Texas 77030

Abstract

Nanoparticles with gold shell and iron core have unique optical and magnetic properties which can be utilized for simultaneous detection and treatment strategies. Several nanoparticles have been synthesized and shown to mediate a variety of potential applications in biomedicine, including cancer molecular optical and magnetic resonance imaging, controlled drug delivery, and photothermal ablation therapy. However, to be effective, these nanoparticles must be delivered efficiently into their targets. In this review, we will provide an updated summary of the gold-shelled magnetic nanoparticles that have been synthesized, methods for characterization, and their potential for cancer diagnosis and treatment. We will also discuss the biological barriers that need to be overcome for the effective delivery of these nanoparticles. The desired nanoparticle characteristics needed to evade these biological barriers were also explained. Hopefully, this review will help researchers in designing nanoparticles by carefully choosing the optimum size, shape, surface charge, and surface coating.

Introduction

Gold-shelled core-shell magnetic nanomaterial is composed of a magnetic core, such as magnetite (Fe_3O_4) or maghemite ($\gamma\text{-Fe}_2\text{O}_3$), coated with a layer of a gold shell. These unique nanostructures are of special interest not only because gold stabilizes (by preventing aggregation) and reduces the toxicity of iron oxide core, but also because of these nanostructures' potential application in diagnostics and therapy.^{1–3} Gold nanostructures possess unique physical and chemical properties, one of the most fascinating aspects being their strong absorption of light in the visible and near-infrared (NIR) region. The origin of this absorption is attributed to collective conduction band electron oscillation in response to the electrical field of the electromagnetic radiation of light. Termed “surface plasmon,” this optical absorption is strongly dependent on the shape and size of the nanostructure. By coating gold on the surface of the iron oxide core, it is possible to tune these nanoparticles to absorb light in the NIR region. The tunable optical properties of gold nanostructures are highly desired for many applications that rely on light absorption, including imaging and therapy. Other attractive features of gold-shelled magnetic nanostructures include easy reductive preparation, high chemical stability, biocompatibility, and affinity for binding to amine and thiol terminal groups in organic molecules. While the gold shell offers distinct optical properties, the magnetic iron oxide core provides the potential for noninvasive imaging using magnetic resonance imaging (MRI) for therapeutic heating in the presence of an alternating magnetic field (please see Lin's article in this issue) and for directing nanoparticles to tumors using an external magnetic field.

Address correspondence to: Chun Li, PhD, Department of Experimental Diagnostic Imaging, Unit 59, The University of Texas M. D. Anderson Cancer Center, 1515 Holcombe Boulevard, Houston, Texas 77030. Phone: (713) 792-5182. Fax: (713) 794-5456. cli@di.mdacc.tmc.edu.

Thus, by combining the magnetic property of the iron oxide core and the optical properties of the gold shell, the multifunctional gold-shelled magnetic nanostructures can potentially find applications in multimodal imaging, therapeutic combinations such as drug delivery and photothermal therapy, and image-guided, minimally invasive intervention.

One of the major challenges for the *in vivo* application of gold-shelled magnetic nanostructures is the delivery of these nanoparticles. The efficacy of most of these systems is often compromised due to the presence of biological barriers. These biological barriers (Table 1) must be overcome for these nanoparticles to reach their target, such as tumors. When nanoparticles are introduced, depending on their physicochemical properties, they are taken up either by liver and spleen, or kidneys, as the major clearance routes. Once they are able to evade clearance, nanoparticles that are targeted to the tumors must be able to pass the tumor vascular pores and be able to disperse in the perivascular area. To increase effectiveness of gold-shelled magnetic nanostructures, their physicochemical properties have to be carefully controlled. These properties include size, shape, morphology, charge, and surface chemistry. Aside from the physicochemical characteristics of the nanoparticle, the innate property of diseased tissues, such as tumor, can be utilized to enhance the uptake of the nanoparticle into the target tissues. For example, tumors have abnormal lymphatic system and leaky vasculature. Because of this, nanoparticles having small particle size can pass and concentrate into the tumor through enhanced permeability and retention effect (passive targeting). In some tumors, there is an increased amount of markers, such as epidermal growth factor receptors and melanocortin receptors. Peptides and antibodies which can directly attach to these receptors may be conjugated on the surface of the NP to target and increase the residence time within the tumors (active targeting). Table 1 summarizes the different biological barriers and the desired nanoparticle characteristics to overcome these barriers.

Here, we will discuss work on the synthesis and characterization of gold-shelled magnetic nanostructures. We will present their potential in cancer diagnosis and therapy and the challenges associated with the development of these techniques. Several review papers have discussed the synthesis and characterization of the iron oxide core and core-shell magnetic nanoparticles.^{4,5}

Synthesis and Characterization

Gold can be coated onto magnetic nanoparticles through reactions in microemulsion, redox transmetalation, iterative hydroxylamine seeding, or other methods.^{4,6} Controlling the size and shape of the nanoparticles is important in order to tune the optical resonance wavelength at the NIR region. The NIR light is desired because this is the region of the electromagnetic spectrum in which absorption of water and naturally occurring fluorochromes is the lowest.⁷ Therefore, NIR light can penetrate deeper into tissues than visible or ultraviolet light without harmful effects to normal, healthy tissues.

Several groups have attempted the synthesis of gold-shelled superparamagnetic iron oxide (SPIO)-containing magnetic nanostructures having plasmon absorption in the NIR region (Table 2). Kim et al.⁸ synthesized a nanostructure with a silica core, a gold shell, and a layer of SPIO sandwiched between silica and gold. The synthesis involves three stages: formation of SPIO-coated silica, nucleation (i.e., small “seed” formation), and growth. Thus, 100-nm silica spheres were first synthesized using the Stöber¹ method. They were then covalently attached to SPIO nanospheres and then functionalized with amine so that the gold will attach on the surface. Then, the gold was allowed to seed and form a thin shell. A complete 15-nm thick gold shell was formed in the last step. Similarly, Stoeva et al.¹⁰ and Salgueirino-Maceira et al.¹¹ synthesized structured gold nanoshells embedded with silica-stabilized magnetite nanoparticles. More recently, Chen et al.¹² reported a sandwich-like nanostructure composed

of a magnetic silica core, an outer silver shell, and a thin layer of gold between the silica and the silver. Nanorice is another gold-coated magnetic nanoparticle, shaped like rice, that absorbs at the NIR region. These nanostructures display two distinct absorptions observed coming from transverse and longitudinal plasmons. The shorter wavelength is about 860 nm, while the longer wavelength is at 1160 nm.¹³ In addition to silica, other dielectric materials interfacing the iron oxide cores and gold shells also were used to fabricate gold-shelled magnetic nanostructures. Wang et al.¹⁴ synthesized a gold-shelled Fe₃O₄ nanostructure with a polymer layer, poly (allylamine hydrochloride), interfacing Fe₃O₄ nanoparticle and the gold shell. Lim et al.¹⁵ synthesized yolk-shell-structured gold nanoparticles that contain SPIO in the core and water as the dielectric interface.

All of the syntheses of the gold-shelled magnetic nanoparticles, with the exception of the yolk-shell-structured gold nanoparticles, have an average diameter of 120 nm or greater.¹⁰⁻¹⁴ It has been previously shown that the cell uptake of gold nanoparticles is dependent on size, with 50 nm being the optimal size.¹⁶ Moreover, smaller nanoparticles are expected to have a better chance to extravasate or pass through tumor vasculature. Thus, it is desirable to have particles with sizes smaller than 100 nm. To meet these needs, we developed gold-shelled silica nanoparticles with SPIO embedded in silica (SPIO@silica-Au).² These nanoparticles had an average diameter of ~80 nm, strong absorption at the NIR region, and high T_2 relaxivity value.¹⁷ Relaxivity values in MRI is the numeric quantification of how much a certain agent can change the relaxation time of the proton in water molecules. Since water molecules are predominant in biological systems, the higher the relaxivity value, the better the contrast that is seen in the MR images. Schema 1 shows the synthesis scheme for SPIO@silica-Au nanoparticles.

The well-known Mie theory has explained the surface plasmon absorption on the basis of classical electrodynamics.¹⁸ The plasmon resonance frequency of core-shelled gold nanostructures is determined by the relative sizes of the inner radius (r_1) and outer radius (r_2) of the gold shell as well as the composition of each component of the nanostructures.¹⁹ The optical absorption and scattering efficiencies of gold nanoshells can be calculated using a computer code employing Mie scattering for concentric sphere geometry.²⁰

As with other nanomaterials, proper structural determination is critical for understanding the properties and functions of gold-shelled magnetic nanostructures. A number of powerful techniques have been employed, including x-ray diffraction (XRD), x-ray absorption spectroscopy (XAS), x-ray absorption near-edge structure (XANES), scanning electron microscopy, transmission electron microscopy (TEM), energy-dispersive x-ray spectroscopy, dynamic light scattering, Fourier transform infrared (FTIR), Raman, and ultraviolet-visible spectroscopy.^{11·14·21·22} XRD is used for determining the crystal structure of crystalline materials. Other x-ray-based spectroscopies are useful in determining the chemical composition of materials. TEM is a high-resolution structural and chemical characterization tool. It can be used to characterize nanoparticles to gain information about particle size, size distribution, shape, crystallinity, and aggregation formation. High-resolution TEM has the capability to image materials at a length scale from atoms (a fraction of a nanometer) to hundreds of nanometers. It is often necessary to use a combination of analytical tools to fully characterize core-shell structured nanoparticles. For example, while it is difficult to distinguish γ -Fe₂O₃ from Fe₃O₄ using only XRD data, XANES or XAS offers a powerful means to distinguish the iron oxide species.²² Another example is the distinction between so called “core-shell” structures versus ‘aggregates’, which are formed from the reaction of HAuCl₄ and Na₂S.²³

The superconducting quantum interference device is a popular technique used to measure magnetic properties of superparamagnetic nanoparticles. The measured saturation moment per

gram (M_{sat}) for core-shell magnetic nanostructures is often lower than that of the corresponding naked superparamagnetic nanoparticles due to the increase of the mass per magnetic nanoparticles caused by the gold-shell coating.^{11,14,22,24} The reversibility of magnetic hysteresis loops (magnetization M versus field H curve) is often used to determine whether superparamagnetic properties of iron oxide are maintained in the core-shell magnetic nanostructures.

Pharmacokinetics, Biodistribution, and Tumor Targeting

Nanoparticles in general may accumulate in the target tissues through two mechanisms: passive targeting and active targeting. Passive targeting is the nonspecific accumulation of nanoparticles in the cells of the RES or in the tumors owing to the innate physiological properties of these tissues. Most nanoparticles are rapidly recognized as foreign and are taken up by the liver and the spleen after they are introduced into the body. SPIO nanoparticles that are efficiently taken up by the liver are therefore suitable imaging agents for liver cancer. Indeed, dextran-coated SPIO or Ferumoxide is the first organ-specific MRI contrast agent approved for clinical applications in detecting and evaluating liver lesions.²⁵ Dextran is a type of sugar that is used to coat the surface of the SPIO to enhance the delivery into the target tissues and prevent the aggregation of the SPIO. On the other hand, to direct nanoparticles to organs other than the liver and the spleen, it is highly desirable that they avoid RES uptake and thus have a prolonged blood circulating time.²⁶ Long-circulating nanoparticles have shown increased accumulation in tumors owing to an enhanced permeability and retention effect, a phenomenon attributed to leaky tumor vasculature and impaired lymphatic drainage system in the tumors.^{27,28}

To date, there is limited study on the pharmacokinetic and biodistribution of gold-shelled magnetic nanostructures.²⁹ However, much *in vivo* data of a variety of gold nanoparticles are available. Critical analysis of these data may help in designing gold-shelled magnetic nanostructures with desired pharmacokinetic properties. In general, physicochemical properties of nanoparticles such as size, shape, morphology, charge, and surface chemistry all affect their pharmacokinetics and biodistribution. The size of the nanoparticles should be small enough to avoid uptake by cells of the RES and big enough to avoid rapid renal clearance. It has been shown that after intravenous injection into rats, spherical gold nanoparticles ranging from 10 to 250 nm in diameter have been taken up primarily by the liver and spleen, with the 10-nm nanoparticles more broadly distributed in various organs.³⁰ Very small particles can easily pass through the leaky capillary wall in the tumor but can easily be pushed out from the tumor by blood.³¹ Therefore, small particles may have good permeability but poor retention. Very big particles, on the other hand, are sequestered easily by RES, and penetration into the leaky vasculature is restricted. In addition to size, the shape and flexibility of the nanoparticles³² and the surface charge play a critical role in blood half-lives of nanoparticles.^{33,34} Positively charged coatings tend to nonspecifically stick to cells.³³ A strong negative charge on the particle surface is also detrimental because of increased liver uptake due to sequestration by phagocytes.³⁵ Therefore, it is generally agreed that nanoparticles with a neutral surface experience extended blood circulation times.³⁶ Since the passive diffusion of the nanoparticle to tumors is dominated by the pore cutoff size of the tumor blood vessels, smaller nanoparticles as compared to larger nanoshells have the advantage in crossing the tumor vessel wall. This is particularly true for such tumors as glioma (brain cancer) and ovarian cancer that have a small pore cutoff size of 7–100 nm.^{37,38}

Surface coating is another factor that greatly affects the pharmacokinetics and biodistribution of nanoparticles. Plasma proteins in blood adsorb onto the surface of bare gold nanoparticles, producing large aggregates³⁹ that may result in altered pharmacokinetics and biodistribution of gold nanoparticles.⁴⁰ Recent work indicates that gold nanospheres, nanoshells, and nanorods

coated with poly(ethylene glycol) (PEG) exhibit prolonged circulation time *in vivo* upon systemic injection.^{41,42} After intravenous injection into rats, various coatings, such as PEG, are found to minimize nonspecific adsorption of proteins onto nanoparticles and to reduce their uptake by the liver.⁴⁰ These coatings, especially PEG, forms a hydrophilic, dense shell that provides the nanoparticle stealth character with minimal non-specific interaction with other proteins. For example, 30-nm PEG-coated gold nanoparticles have been successfully used to deliver proteins, such as tumor necrosis factor to solid tumors.⁴² PEG-coated gold nanoparticles also have been reported to be promising computed tomography (CT) contrast agents for blood pool imaging because they exhibit a longer blood circulation time and a 5.7 times higher attenuation than iodine-based CT contrast agents that are currently used.^{43,44} Qian et al.⁴⁵ described the use of PEGylated gold nanoparticles for *in vivo* tumor targeting and molecular imaging based on their surface-enhanced Raman scattering effect. In a recent study done in our laboratory, we found that the length of PEG attached on the surface of the gold, the method of attaching PEG, and the size of the core coated with PEG affect the pharmacokinetics and biodistribution of these nanoparticles.⁴⁶

Active targeting is a ligand-directed, site-specific accumulation of nanoparticles. By conjugating targeting molecules that possess high affinity toward unique molecular signatures found in malignant cells, these nanoparticles accumulate more efficiently and stay longer in tumors. Researchers have attempted to attach tumor-cell specific “address tags” such as antibodies^{3,24,47,48} or peptides⁴⁹ to gold-shelled nanostructures. For example, the antihuman epidermal growth factor receptor 2 (HER2) antibody was conjugated onto the surface of gold-shelled iron oxide nanoparticles and was shown *in vitro* to target and mediate killing of tumor cells through photothermal ablation therapy.²⁴ Photothermal ablation therapy is a type of therapy which utilizes agents, such as nanoparticles which absorb light at a particular wavelength, converts the absorbed light into heat, and the heating causes death in cells. In two separate publications, we have previously conjugated an antiepidermal growth factor receptor monoclonal antibody C225 and melanocyte stimulating hormone (MSH) peptide, on the surface of much smaller hollow gold nanospheres ~40 nm in diameter. Our results show that C225-conjugated gold nanoparticles could effectively target cells that have increased amounts of epidermal growth factor receptors, such as in tumors, and mediate laser-induced photothermal ablation therapy *in vitro*.³ However, only a moderate increase in tumor uptake of targeted nanoparticles was observed *in vivo*. This may be due to the size of the antibody that is coated on the surface of NP, which makes it difficult to reach the target site. After this study, a much smaller MSH peptide directed at melanocortin receptors was used as a targeting ligand. Melanocortin is an important marker for melanoma and our results showed a significantly higher tumor accumulation was achieved *in vivo* with peptide-conjugated hollow gold nanospheres than without the peptide.⁴⁹ To summarize the results of these two studies, nanoparticle size is not the only factor that that can be important in determining the efficiency of targeted delivery of gold nanostructures but also the the size of the targeting ligand attached on the surface of the nanoparticle.

Applications in Cancer Diagnosis and Therapy

The premise of gold-shelled magnetic nanostructures is their multifunctionality for targeted delivery, diagnosis, imaging guidance, and photothermal ablation therapy. Applications in surface-enhanced Raman scattering⁵⁰ and photoacoustic imaging^{51,52} based on the optical properties of this novel nanostructure are possible, but no study has been reported thus far. Here, we briefly discuss the potential applications of gold-shelled magnetic nanostructures in MRI and thermal ablation therapy.

MRI is a noninvasive technique used to obtain anatomic and functional information with high spatial and temporal resolution (please see Lin’s article in this issue). MRI measures changes

in the magnetization of hydrogen protons in water molecules placed in a magnetic field after a pulse of radiofrequency has hit them. Protons from different tissues relax at different rates, resulting in clearly defined anatomical images. In clinical settings, a contrast agent is often necessary to differentiate between normal and abnormal tissues. Signal intensity arises largely from the local values of the longitudinal relaxation rate of water protons, $1/T_1$, and the transverse rate, $1/T_2$. Pulse sequences that emphasize changes in $1/T_2$ are referred to as T_2 -weighted scans, the signal of which decreases with increasing $1/T_2$. Iron oxide nanoparticles are used to enhance T_2 -weighted images owing to their large transverse relaxivity values (r_2 , refer to the amount of increase in $1/T_2$ per millimolar of contrast agent) and large r_2/r_1 ratio, where r_1 refers to the amount of increase in $1/T_1$ per millimolar of contrast agent. To date, a wide variety of particles have been produced, differing in size (hydrodynamic particle size varying from 10 to 500 nm) and type of coating material used (such as dextran, starch, albumin, silicones, PEG).⁵³ An extensive review on the imaging applications of magnetic iron oxide nanoparticles has been published recently (please also see Lin's article in this issue).⁶

Several gold-shelled iron oxides nanoparticles showed favorable transverse relaxivity.^{8,21,24} For example, SPIO@silica-Au nanoshells exhibited high transverse relaxivity, r_2 , and a large r_2/r_1 ratio and therefore could be imaged by MRI to obtain T_2 -weighted images.²¹ Preliminary *in vivo* data show that these nanoparticles mediated efficient photothermal effect in nude mice implanted with tumor due to its strong absorption in the NIR region, while the presence of SPIO provided contrast in T_2^* MR imaging (Figure 1).²⁹ T_2^* is a type of MR imaging that is acquired quicker than a T_2 -weighted and can be quantified using a mathematical algorithm. These data suggest that dual functional SPIO@silica-Au may be used in both therapeutic and diagnostic (theranostic) applications in which the intratumoral distribution of the nanoparticles depicted by MRI may be used to assist planning of photothermal therapy and prediction of the treatment outcome.

The use of heat to preferentially kill cancer cells is a promising approach to cancer therapy. Depending on the temperature achieved, either hyperthermia or thermal ablation is ensured. Hyperthermia is the heating of tissues to 42 to 46°C,⁵⁴ while thermal ablation occurs when tissues are heated to temperatures greater than 46°C.⁵⁵ This type of heating causes denaturation of proteins which in turn results in cellular inactivation by inducing and regulating apoptosis (programmed cell death), signal transduction and multidrug resistance. Repeatedly heating tissues to hyperthermic temperatures signals the release of heat shock proteins.⁵⁶ Hyperthermia also can boost the efficacy of radiotherapy^{57,58} and chemotherapy.⁵⁹ Thermal ablation kills cells directly by inducing necrosis.⁶⁰ Hyperthermia/thermal ablation is attractive because it is a physical treatment and therefore should have fewer side effects compared with conventional cancer treatments. This form of treatment also may be performed repeatedly without the accumulation of toxic side effects. There are two major ways in which hyperthermia/thermal ablation can be induced with the introduction of gold-shelled magnetic nanoparticles. The first is when NIR light is absorbed to generate a photothermal effect, and the second is when the magnetic core is activated in the presence of an alternating magnetic field.

Laser-induced photothermal ablation therapy utilizes the plasmon absorption by gold nanoparticles of NIR light. The absorbed light energy is converted into thermal energy, which ultimately destroys cancer cells. To be effective, the plasmon absorption of the gold-shelled magnetic nanostructures should be tuned to the NIR region that matches the wavelength of the laser light. An aqueous solution of SPIO@silica-Au nanoshells showed an increase in temperature of 16°C at a concentration of 7.5×10^{12} particles/mL when irradiated with 810 nm of continuous-wave diode laser at 1 W for 15 min. This increase in temperature is concentration-dependent.¹⁷ Selective ablation of tumors cells treated with targeted gold-shelled magnetic nanostructures and NIR laser has been demonstrated *in vitro*.^{8,24} However,

no data have been published indicating the efficacy of this type of agent *in vivo* after systemic administration.

A magnetic particle can generate heat by hysteresis loss. This concept of mediating hyperthermia using a magnetic material was first proposed by Gilchrist⁶¹ in 1957. Two years after they published their work on *ex vivo* magnetic fluid hyperthermia, Gilchrist and co-workers performed successful hyperthermia experiments on lymph nodes of rats and dogs.^{62, 63} To find the most effective treatment based on magnetic materials, Gordon et al.⁶⁴ proposed the concept of intracellular hyperthermia by using submicron magnetic particles capable of penetrating the cell membrane. This technique resulted in selective thermal destruction of cancer cells upon the application of an external high-frequency or pulsed electromagnetic field, with little effect on normal cells. Again, a prerequisite for successful electromagnetic field-mediated destruction of tumor cells is efficient and selective uptake of magnetic nanoparticles in the tumor cells. Although experiments on the heat-generating capacity of gold-shelled magnetic nanostructures under alternating magnetic field have not been reported, it is anticipated that this type of nanoparticle could mediate the thermal ablation effect using both an NIR laser and an alternating magnetic field, making it feasible to treat both deep and superficial cancer lesions.

Summary and Outlook

Photothermal ablation therapy mediated by gold nanoparticles is a new minimally invasive therapeutic approach that has been shown *in vitro* and *in vivo* to be highly effective at killing tumor cells. Effective gold-based photothermal ablation therapy in the clinical setting will require selective delivery of a sufficient amount of gold nanoshells to tumors to mediate a photothermal effect. In addition, techniques must be developed to enable accurate pretreatment thermal dose calculation and noninvasive real-time monitoring of the spatiotemporal temperature profile and response to therapy in a given local target volume. Multifunctional gold-shelled magnetic nanoparticles, with their combination of unique magnetic and optical properties, should enhance the efficacy of gold nanoshell-mediated photothermal therapy by making it possible to direct more nanoparticles to tumors through the application of external magnetic fields and by permitting real-time *in vivo* MRI of the distribution of the nanoparticles before, during, and after photothermal therapy. However, with the exception of two recent reports with hollow gold nanospheres,^{3,49} active targeting of NIR-absorbing gold-shelled magnetic nanoparticles to tumors as MRI-visible thermal coupling agents has not been demonstrated *in vivo*. Successful targeted delivery of these nanostructures *in vivo* requires overcoming a number of biological barriers, including RES uptake, extravasation into extravascular fluid space, and dispersion into the tumor matrix. Meeting these challenges requires an in-depth understanding between the physiochemical characteristics, particularly the surface properties of these nanoparticles, and their *in vivo* behaviors. In the ideal case, nanostructures with an absorption band tunable in the NIR region, small size (< 50 nm), uniform size distribution, and high colloidal stability are preferred. Fabrication of such nanostructures remains a significant challenge for synthetic chemists.

To date, most research stands on the proof-of-concept stage. Detailed preclinical studies should be addressed, especially to pharmacokinetics and *in vivo* tumor targeting and therapeutic effect. Furthermore, the metabolism of the gold nanoparticles as well as acute and long-term clearance and long-term toxicity need to be examined thoroughly, although preliminary studies suggest that gold nanoparticles have excellent biocompatibility.

Acknowledgments

This work is supported by the National Cancer Institute (grant R01 CA119387) and by the John S. Dunn Foundation.

References

1. Jain PK, Huang X, El-Sayed IH, El-Sayed MA. *Acc Chem Res.* May 1;2008
2. Daniel MC, Astruc D. *Chem Rev* 2004;104(1):293. [PubMed: 14719978]
3. Melancon MP, Lu W, Yang Z, Zhang R, Cheng Z, Elliot AM, Stafford J, Olson T, Zhang JZ, Li C. *Mol Cancer Ther* 2008;7(6):1730. [PubMed: 18566244]
4. Lu AH, Salabas EL, Schuth F. *Angew Chem Int Ed Engl* 2007;46(8):1222. [PubMed: 17278160]
5. Tartaj P, Morales MDP, Veintemillas-Verdaguer S, Gonzalez-Carreno T, Serna CJ. *J Phys D: Appl Phys* 2003;36(13):R182.
6. Laurent S, Forge D, Port M, Roch A, Robic C, Vander Elst L, Muller RN. *Chem Rev* 2008;108(6):2064. [PubMed: 18543879]
7. Mahmood U, Weissleder R. *Mol Cancer Ther* 2003;2(5):489. [PubMed: 12748311]
8. Kim J, Park S, Ji EL, Jin SM, Lee JH, Lee IS, Yang I, Kim JS, Kim SK, Cho MH, Hyeon T. *Angew Chem Int Ed* 2006;45(46):7754.
9. Stöber W, Fink A, Bohn E. *J Colloid Interface Sci* 1968;26(1):62.
10. Stoeva SI, Huo F, Lee JS, Mirkin CA. *J Am Chem Soc* 2005;127(44):15362. [PubMed: 16262387]
11. Salgueirino-Maceira V, Correa-Duarte MA, Farle M, Lopez-Quintela A, Sieradzki K, Diaz R. *Chem Mater* 2006;18(11):2701.
12. Chen M, Kim YN, Lee HM, Li C, Cho SO. *J Phys Chem C* 2008;112(24):8870.
13. Wang H, Brandl DW, Le F, Nordlander P, Halas NJ. *Nano Lett* 2006;6(4):827. [PubMed: 16608292]
14. Wang L, Bai J, Li Y, Huang Y. *Angew Chem Int Ed Engl* 2008;47(13):2439. [PubMed: 18278779]
15. Lim IS, Njoki PN, Park HY, Wang X, Wang L, Mott D, Zhong CJ. *Nanotechnology* 2008;19:1. [PubMed: 19436766]
16. Thorek DL, Tsourkas A. *Biomaterials* 2008;29(26):3583. [PubMed: 18533252]
17. Ji X, Shao R, Elliott AM, Stafford RJ, Esparza-Coss E, Bankson JA, Liang G, Luo ZP, Park K, Markert JT, Li C. *J Phys Chem C* 2007;111(17):6245.
18. Mie G. *Ann Phys* 1908;25:377.
19. Averitt RD, Sarkar D, Halas NJ. *Phys Rev Lett* 1997;78(22):4217.
20. Charamisinau I, Happawana G, Evans G, Rosen A, Hsi RA, Bour D. *Appl Opt* 2004;44(24):5055. [PubMed: 16121790]
21. Ji X, Shao R, Elliott AM, Stafford RJ, Esparza-Coss E, Bankson JA, Liang G, Luo ZP, Park K, Markert JT, Li C. *J Phys Chem C* 2007;111(17):6245.
22. Park K, Liang G, Ji X, Luo ZP, Li C, Croft MC, Markert JT. *J Phys Chem C* 2007;111(50):18512.
23. Schwartzberg AM, Grant CD, van Buuren T, Zhang JZ. *J Phys Chem C* 2007;111(25):8892.
24. Lim YT, Cho MY, Kim JK, Hwangbo S, Chung BH. *Chembiochem* 2007;8(18):2204. [PubMed: 17957817]
25. Hamm B, Staks T, Taupitz M, Maibauer R, Speidel A, Huppertz A, Frenzel T, Lawaczeck R, Wolf KJ, Lange L. *J Magn Reson Imaging* 1994;4(5):659. [PubMed: 7981510]
26. Li SD, Huang L. *Mol Pharm* 2008;5(4):496. [PubMed: 18611037]
27. Maeda H, Wu J, Sawa T, Matsumura Y, Hori K. *J Control Release* 2000;65(1–2):271. [PubMed: 10699287]
28. Li C. *Adv Drug Deliv Rev* 2002;54(5):695. [PubMed: 12204599]
29. Melancon, MP.; Elliot, A.; Shetty, A.; Taylor, B.; Ji, X-J.; Huang, Q.; Gelovani, J.; Stafford, J.; Li, C. 2008 World Molecular Imaging Congress; Sept. 10–13, 2008; Nice, France. 2008.
30. De Jong WH, Hagens WI, Krystek P, Burger MC, Sips AJ, Geertsma RE. *Biomaterials* 2008;29(12):1912. [PubMed: 18242692]
31. Choi HS, Liu W, Misra P, Tanaka E, Zimmer JP, Itty Ipe B, Bawendi MG, Frangioni JV. *Nat Biotechnol* 2007;25(10):1165. [PubMed: 17891134]
32. Decuzzi P, Ferrari M. *Biomaterials* 2006;27(30):5307. [PubMed: 16797691]
33. Fujita T, Nishikawa M, Ohtsubo Y, Ohno J, Takakura Y, Sezaki H, Hashida M. *J Drug Target* 1994;2(2):157. [PubMed: 8069594]

34. Papisov MI, Bogdanov A Jr, Schaffer B, Nossiff N, Shen T, Weissleder R, Brady TJ. *J Magn Magn Mater* 1993;122(1–3):383.
35. Chouilly C, Pouliquen I, Lucet JJ, Jeune P, Jallet P. *J Microencapsul* 1996;13:245. [PubMed: 8860681]
36. Sun C, Lee JSH, Zhang M. *Adv Drug Deliv Rev* 2008;60(11):1252. [PubMed: 18558452]
37. Hobbs SK, Monsky WL, Yuan F, Roberts WG, Griffith L, Torchilin VP, Jain RK. *Proc Nat Acad Sci USA* 1998;95(8):4607. [PubMed: 9539785]
38. Kong G, Braun RD, Dewhirst MW. *Cancer Res* 2000;60(16):4440. [PubMed: 10969790]
39. Zhang F, Skoda MW, Jacobs RM, Zorn S, Martin RA, Martin CM, Clark GF, Goerigk G, Schreiber F. *J Phys Chem A* 2007;111(49):12229. [PubMed: 17914772]
40. Otsuka H, Nagasaki Y, Kataoka K. *Adv Drug Deliv Rev* 2003;55(3):403. [PubMed: 12628324]
41. Niidome T, Yamagata M, Okamoto Y, Akiyama Y, Takahashi H, Kawano T, Katayama Y, Niidome Y. *J Control Release* 2006;114(3):343. [PubMed: 16876898]
42. Paciotti GF, Myer L, Weinreich D, Goia D, Pavel N, McLaughlin RE, Tamarkin L. *Drug Deliv* 2004;11(3):169. [PubMed: 15204636]
43. Hainfeld JF, Slatkin DN, Focella TM, Smilowitz HM. *Br J Radiol* 2006;79(939):248. [PubMed: 16498039]
44. Kim D, Park S, Lee JH, Jeong YY, Jon S. *J Am Chem Soc* 2007;129(24):7661. [PubMed: 17530850]
45. Qian X, Peng XH, Ansari DO, Yin-Goen Q, Chen GZ, Shin DM, Yang L, Young AN, Wang MD, Nie S. *Nat Biotechnol* 2008;26(1):83. [PubMed: 18157119]
46. Zhang G, Yang Z, Lu W, Zhang R, Huang Q, Tian M, Li L, Liang D, Li C. *Biomaterials*. 2009
47. Lowery AR, Gobin AM, Day ES, Shah KY, Halas NJ, West JL. *Clin Cancer Res* 2005;11(24):9097s.
48. Chen JY, Wang DL, Xi JF, Au L, Siekkinen A, Warsen A, Li ZY, Zhang H, Xia YN, Li XD. *Nano Lett* 2007;7(5):1318. [PubMed: 17430005]
49. Lu W, Xiong C, Zhang G, Huang Q, Zhang R, Zhang JZ, Li C. *Clin Cancer Res* 2009;15(3):876. [PubMed: 19188158]
50. Schwartzberg AM, Oshiro TY, Zhang JZ, Huser T, Talley CE. *Anal Chem* 2006;78:4732. [PubMed: 16808490]
51. Guillon C, Langot P, Del Fatti N, Vallee F, Kirakosyan AS, Shahbazyan TV, Cardinal T, Treguer M. *Nano Lett* 2007;7(1):138. [PubMed: 17212453]
52. Wang YW, Xie XY, Wang XD, Ku G, Gill KL, O'Neal DP, Stoica G, Wang LV. *Nano Lett* 2004;4(9):1689.
53. Babes L, Denizot B, Tanguy G, Le Jeune JJ, Jallet P. *J Colloid Interface Sci* 1999;212(2):474–482. [PubMed: 10092379]
54. Hilger I, Fruhauf K, Andra W, Hiergeist R, Hergt R, Kaiser WA. *Acad Radiol* 2002;9(2):198. [PubMed: 11918373]
55. Hilger I, Andra W, Hergt R, Hiergeist R, Schubert H, Kaiser WA. *Radiology* 2001;218(2):570. [PubMed: 11161180]
56. Milani V, Endres M, Kuppner MC, Issels RD, Noessner E. *Dtsch Med Wochenschr* 2004;129(1–2):31. [PubMed: 14703579]
57. Overgaard J. *Int J Radiat Oncol Biol Phys* 1989;16(3):535. [PubMed: 2646256]
58. Overgaard J, Gonzalez Gonzalez D, Hulshof MC, Arcangeli G, Dahl O, Mella O, Bentzen SM. *Lancet* 1995;345(8949):540. [PubMed: 7776772]
59. Engelhardt R. *Recent Results Cancer Res* 1987;104:136. [PubMed: 3296049]
60. Dewey WC. *Int J Hyperthermia* 1994;10(4):457. [PubMed: 7963805]
61. Gilchrist RK, Medal R, Shorey WD, Hanselman RC, Parrott JC, Taylor CB. *Ann Surg* 1957;146(4):596. [PubMed: 13470751]
62. Gilchrist RK, Shorey WD, Hanselman RC, Depeyster FA, Yang J, Medal R. *Ann Surg* 1965;161:890. [PubMed: 14295940]
63. Medal R, Gilchrist RK, Barker W, Hanselman R. *Arch Surg* 1959;79:427.
64. Gordon RT, Hines JR, Gordon D. *Med Hypotheses* 1979;5(1):83. [PubMed: 459972]

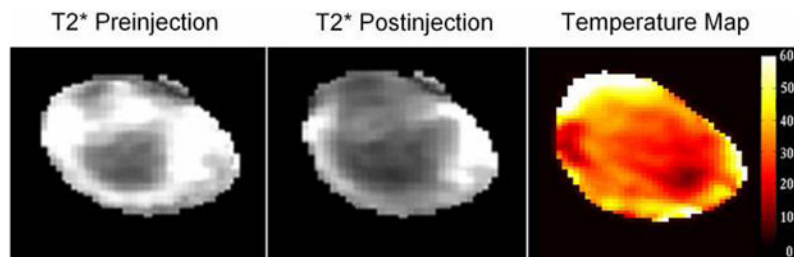
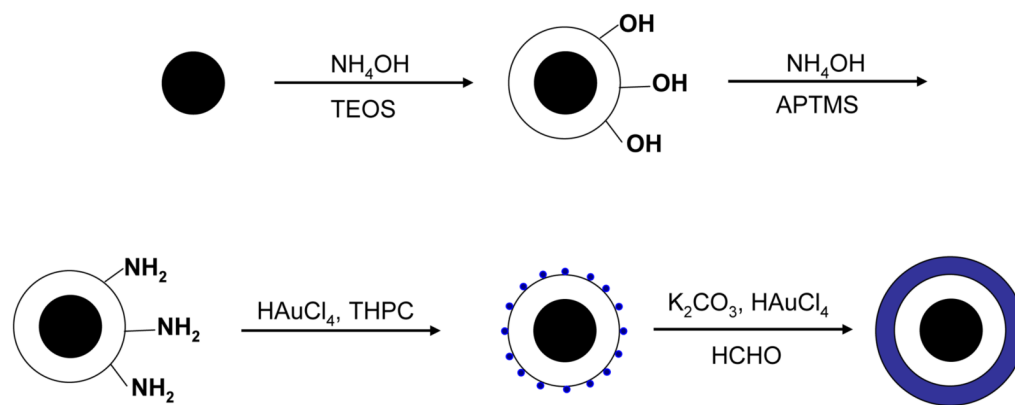


Figure 1.

T2* Magnetic resonance imaging (MRI) and the magnetic resonance temperature (MRTI) map of a subcutaneous A431 tumor injected with SPIO@silica-Au nanoparticles in the tumor at a dose of 1×10^{11} particles/site. Note the darkening of the tumor in T2*-weighted MRI after the injection of the SPIO@silica-Au, and the increase in temperature by as much as 60°C as shown in MRTI. This indicates the potential use of SPIO@silica-Au for the simultaneous MRI and photothermal therapy.

**Scheme 1.**

Synthesis of SPIO@silica-Au nanoshells.¹⁷ Silica-coated superparamagnetic iron oxide (SPIO) ($\gamma\text{-Fe}_2\text{O}_3$) nanoparticles were synthesized using the Stöber process. After the surface of the silica shell was functionalized with 3-aminopropyltrimethoxysilane (APTMS), 2–3 nm gold nanocrystal seeds were attached to the amino groups on the silica sphere by reducing chloroauric acid (HAuCl_4) with tetrakis(hydroxymethyl) phosphonium chloride (THPC). Finally, the attached gold nanoseeds were used to nucleate the growth of a gold overlay on the silica surface to form a gold nanoshell.

Table 1

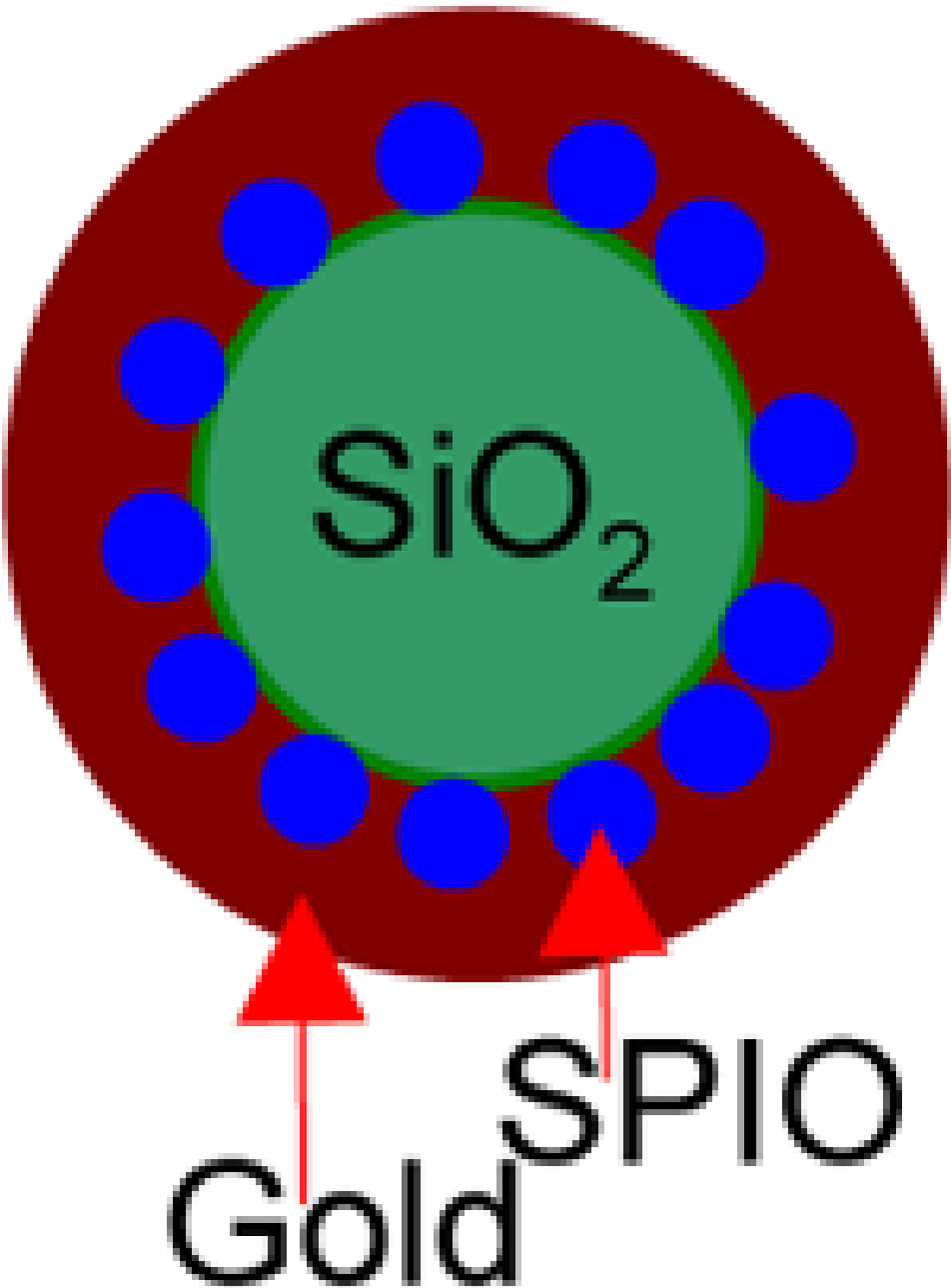
Biological barriers affecting targeting of gold nanoparticles to solid tumors

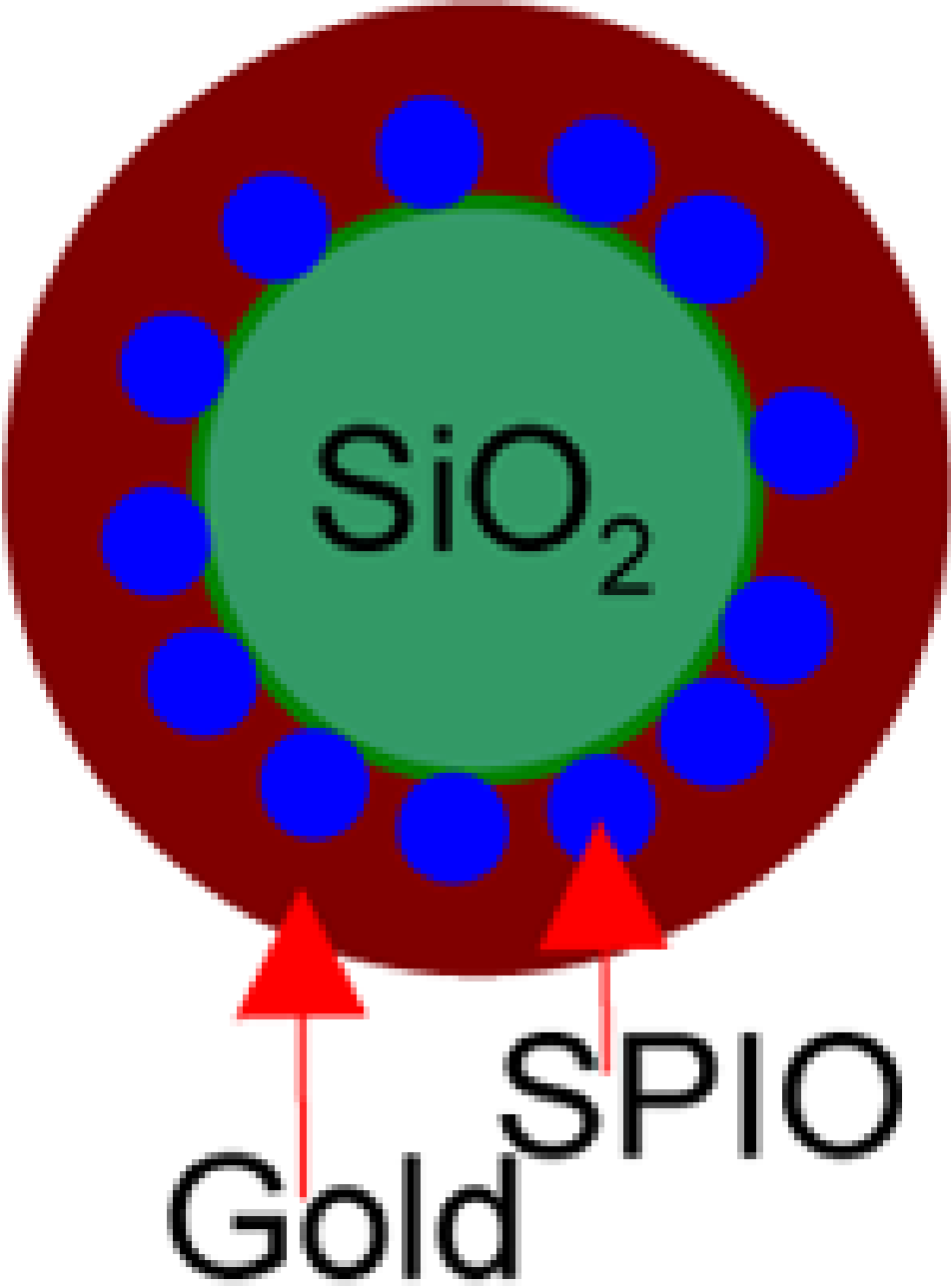
Barriers	Property	Desired NP characteristics to overcome barriers
Liver and Spleen (RES [§])	Clearance by phagocytic uptake and hepatic filtration	≤100 nm NP size and negative or neutral surface charge
Kidney	Clearance through glomerular filtration	≥5 nm in NP size to avoid rapid renal clearance; should, be hydrophilic and neutral
Tumors endothelial lining (tumor vasculature)	Vascular pores (endothelial fenestration) varies from 50 nm to 600 nm in tumors	smaller particle size (<600 nm can pass, ideally <100 nm) to go through the pore
Dispersion from perivascular area	Slow diffusion coefficient for nanoparticles	Active targeting and active transport mechanisms

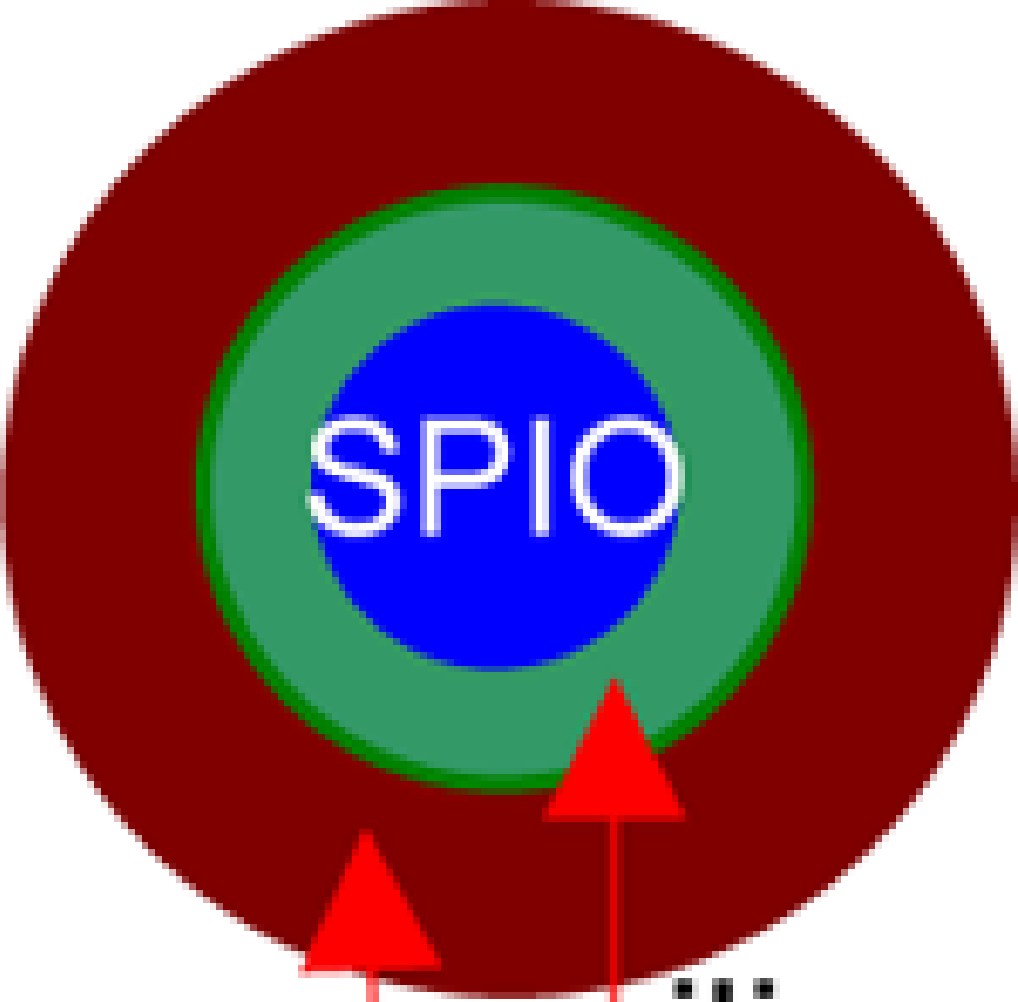
* RES (reticuloendothelial system) is part of the immune system which consists of phagocytic cells, primarily monocytes and macrophages. These cells accumulate in the liver (Kuffner cells), spleen, and lymph nodes.


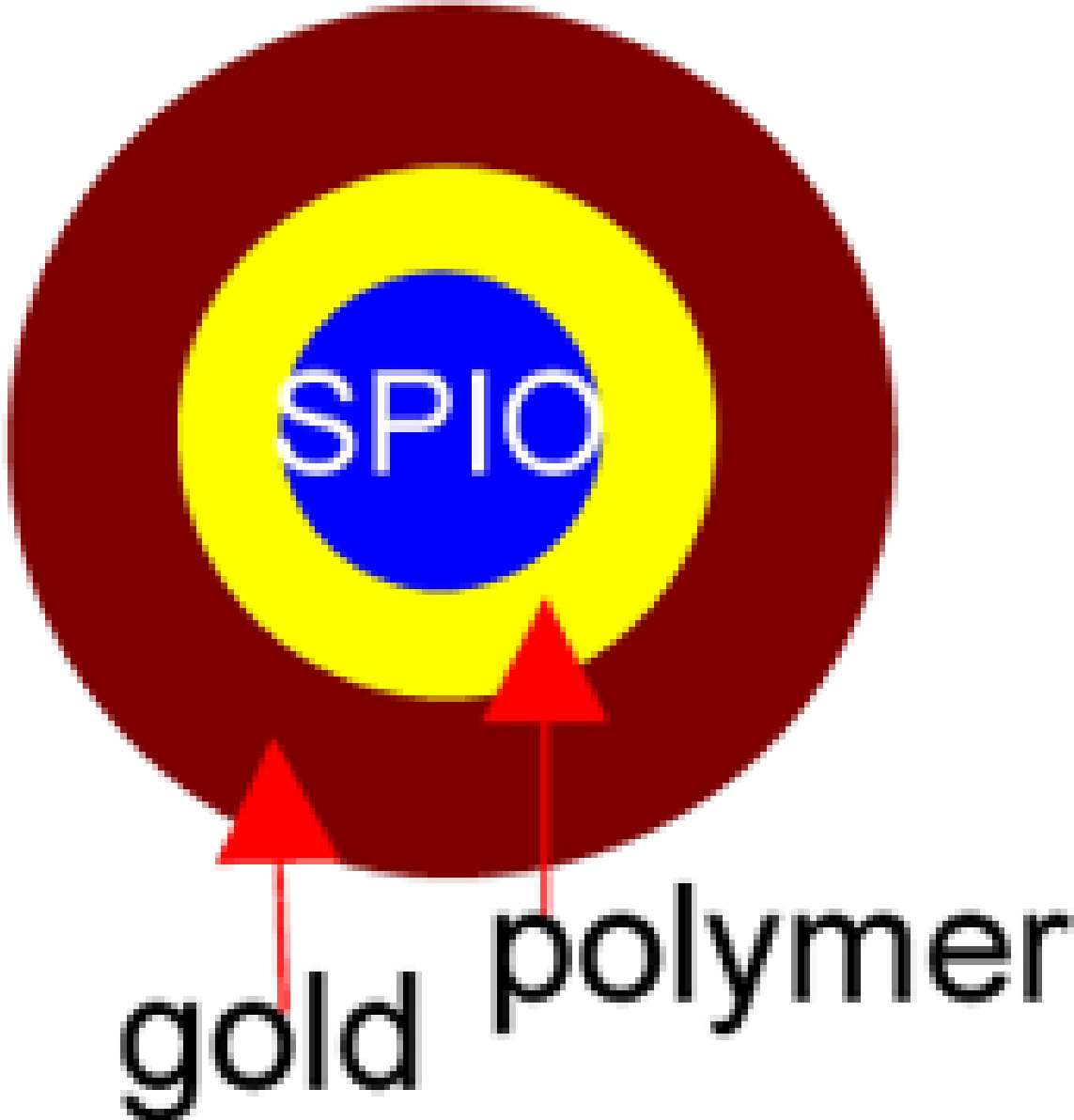
Table 2





Summary of gold-shelled magnetic nanoparticles


Structure	Characteristics	In
	<p>Size: ~120 nm Surface: PEG and anti-HER2/<i>neu</i> Absorbance: 700–900 nm (broad) Magnetic: $r_2 = 251 \text{ nM}^{-1}\text{s}^{-1}$</p>	<p>T_2 M da wi an ne Lo po mV ne cel HE po (S He ne (H mV</p>

Structure	Characteristics	In
 <p>The diagram illustrates a core-shell nanoparticle structure. At the center is a green circle labeled SiO_2. This is surrounded by a ring of blue circles. The entire structure is enclosed within a larger red circle. Below the red circle, two red arrows point upwards towards the structure. The arrow on the left is labeled "Gold" and the arrow on the right is labeled "SPIO".</p>	<p>Size: >200 nm Surface: 3' and 5'-thiol modified DNA Absorbance: 600–900 nm (broad) Magnetic: Movement of NP with a bar of magnet</p>	<p>No</p>

Structure	Characteristics	In
 <p data-bbox="402 1388 748 1566">gold</p> <p data-bbox="821 1266 1227 1409">silica</p>	<p data-bbox="1442 258 1580 516">Size: >200 nm Surface: None Absorbance: can be tuned from visible to NIR Magnetic: Reversible hysteresis loop and movement of NP with a bar of magnet.</p>	<p data-bbox="1604 258 1624 279">No</p>

Structure	Characteristics	In
	<p>Size: ~170 nm Surface: None Absorbance: ~480–1000 nm (broad) Magnetic: Reversible hysteresis loop. Irradiation with 808 nm laser had temperature increase with increasing NP concentration</p>	<p>No</p>
	<p>Size: 273 ± 17.9 nm Surface: None Absorbance: 600–900 nm (broad) Magnetic: Reversible hysteresis loop and movement of sample with a bar of magnet</p>	<p>No</p>

Structure	Characteristics	In
	<p>Size: longitudinal = 340 ± 20 nm; transverse= None 54 ± 4 nm Surface: None Absorbance: 860 nm and 1160</p>	<p>No</p>
	<p>Size: 82.2 ± 9.7 nm Surface: PEG Absorbance: 600–900 nm (broad) Magnetic: Reversible hysteresis loop and movement of NP with a bar of magnet.</p>	<p>No</p>
	<p>Size: ~80 nm Shape: spherical Surface: PEG Absorbance: 600–900 nm (broad) Magnetic: $r_2 =$ $369 \text{ mM}^{-1} \text{ s}^{-1}$</p>	<p>Da ag em wi usi las inc ter of Te inc lin rel po co</p>
	<p>Size: 30.4 ± 4.4 nm Shape: spherical Surface: C225 monoclonal antibody Absorbance: 808 nm (narrow)</p>	<p>Se bin C2 wa wi cel Or tre C2 an las aft no co las tar</p>

Structure	Characteristics	<i>In</i>
	<p>Size: 43.5 ± 2.3 nm Shape: spherical Surface: melanocyte stimulating hormone (MSH) peptide Absorbance: 808 nm (narrow)</p>	<p>Re Se bir M wa in me cel cel wi HG nm aft no co al al tar + 1</p>